Super resolution from diffraction limited images with kernel-phases

Frantz Martinache[a]

[a]Subaru Telescope, 650 N. A'ohoku Place, HI 96720, USA

ABSTRACT

Kernel-phase is a recently developed paradigm to tackle the classical problem of image deconvolution, based on an interferometric point of view of image formation. Kernel-phase inherits and borrows from the notion of closure-phase, especially as it is used in the context of non-redundant Fizeau interferometry, but extends its application to pupils of arbitrary shape, for diffraction limited images. It can therefore readily be (and is being) used to process existing archival data acquired by space borne telescopes (HST/NICMOS) as well as well corrected AO data from ground based telescopes. The additional calibration brought by kernel-phase boosts the resolution of conventional images and enables the detection of otherwise hidden faint features at the resolution limit and beyond, a regime often refered to as super-resolution. Kernel-phase analysis of archival data leads to new discoveries and/or improved relative astrometry and photometry. The paper also presents how the technique may influence the geometry of new interferometric arrays designed for imaging, dusting off a topic that has known little evolution for the past 40 years; and presents hints of a fast solution to the calibration of non-common path errors in AO systems, using direct focal plane based wavefront sensing.

1. INTRODUCTION

Imaging in the high angular resolution regime comes down to solving the problem of deconvolving an unknown object function from an ever changing point spread function (PSF). The development of adaptive optics (AO), now ubiquitous on major ground based observatories, dramatically changed this arena, by turning previously seeing limited images into diffraction limited ones, thus enabling high angular resolution observations on large telescopes. An 8-to-10 meter telescope observing in the H-band (1.6 μm) exhibits a 0.04 arcsecond diffraction limit, sufficient to resolve Jupiter like planets in formation around stars of the nearby young associations Taurus (distance $\sim$ 145 pc).[1,2] The resolving power of an AO-equiped 30-meter class telescope should prove sufficient to image Super-Earth type planets in the habitable zone of the nearby M-dwarfs.

High contrast detections are however currently limited by residual aberrations, responsible for the presence of speckles in the image. Different schemes have been developed to sort out the PSF from the object function in images, and a very successful approach is to use some form of diversity in the PSF: angular differential imaging[3] for instance, uses field-rotation to differentiate true companions from static speckles. Aggressive alternatives are becoming available with updated AO systems, often refered to as extreme-AO systems, with active optics that can be used to introduce phase diversities, for instance creating speckle free regions in the image[4] or estimating the coherence of speckles.[5,6]

This paper presents an alternative approach, based on an interferometric point of view of image formation. The approach builds on the recent development of non-redundant aperture masking interferometry.[7,8] Masking interferometry, first used in 1873 by Stephan in an attempt to measure the angular diameter of stars with the 80-cm baseline of the telescope of the Observatoire de Marseille, was indeed revived after the invention of speckle interferometry,[?] the emergence of large telescopes,[9] and the generalization of AO.[10] One of its most recent application is the detection of high contrast companions around stars, both evolved and young.

Non-redundant masking interferometry takes advantage of the self-calibrating properties of an observable quantity called closure-phase.[11] This remarkable quantity, originally invented in the context of radio astronomy, exhibits a compelling property: it rejects all residual phase errors on the interferometer pupil. At optical wavelength, because it is determined from the analysis of the final science detector, and not estimated from a

email: frantz@naoj.org

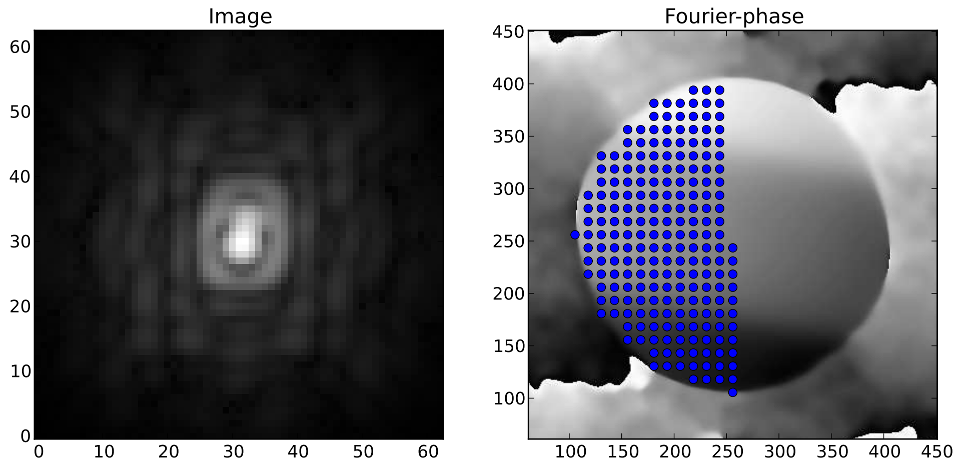

Figure 1. Left: Example of high Strehl image of a barely resolved binary observed with HST/NICMOS in the H band. Right: Phase information contained in the Fourier transform of the same image. Even for features that are barely resolved in the image, the information spreads across the entire uv plane. In blue are highlighted the uv sample points used for the construction of kernel-phases (cf. text).

separate "sensing" channel, it is immune to non-common path errors that are partly responsible for the presence of quasi-static speckles that limit the performance of AO-imaging based planet search programs. Once extracted, the closure phase can then be used as input of a parametric model, for instance of a binary star of variable characteristics (angular separation, position angle and luminosity contrast), to confirm or infirm the presence of a companion around a given source, while uncertainties provide contrast detection limits. Recent discoveries demonstrate sensitivity of over 6 magnitudes in the near-infrared at angular separations ranging from 0.5 to 4 λ/D, which on very young objects is sufficient to make exciting discoveries.[1,2]

It was demonstrated that the notion of closure phase, requiring a strictly non-redundant aperture can be generalized to arbitrarily shaped (i.e. including redundant) pupils, if the wavefront quality is sufficient.[12,13] This generalization of the closure-phase is coined Kernel-phase, since these closure relations form a basis for the null-space (or Kernel) of a linear operator. This paper summarizes some of the ongoing developments that the technique enables. First, Section 2 presents the general theory of kernel-phase, and shows ... benefits over closure phase? Sections 3.1 and 3.2 respectively present recent partial results obtained using kernel-phase data analysis on HST/NICMOS observations of brown dwarfs (Pope et al, in prep) and some results from the analysis of ground based AO data. Section 4 discusses how kernel-phase can lead to the design of better interferometric masks designed for the imaging of complex sources, while Section 5 presents some preliminary results on the wavefront sensing applications of the formalism developed for kernel-phase.

2. KERNEL-PHASE

2.1 The phase transfer matrix

For any imaging system fed with an imperfect wavefront, as long as the wavefront errors remain small, a simple linear model relates the phase errors in the pupil plane, summarized by the vector φ, and the phase measured in the uv plane Φ:

$$\Phi = \Phi_0 + \mathbf{A} \cdot \varphi, \tag{1}$$

where the additional term Φ_0 represents the "true" uv phase of the observed source, and $\mathbf{A}$ is a linear operator, called the phase transfer matrix, and whose properties form the basis of this work. Fig. 1 shows one example of very clear uv-plane phase signature for an otherwise barely resolved binary star. The moderate contrast of the binary and the very high Strehl of the image makes this uv phase signature (Φ_0) visible without any additional treatment. In most cases, the phase information is polluted by pupil phase errors φ. Eq. 1 essentially describes these errors propagate through the optical system modeled by $\mathbf{A}$ and pollute true phase measurements Φ_0. We take advantage that even in the most unfavorable scenario, there is always more information available in the uv plane than in the pupil: the operator $\mathbf{A}$ is always rectangular with more rows than columns, although actual dimensions however entirely depend on the geometry of the pupil. The information brought by these additional rows is used to form kernel-phases.

2.2 Influence of the array geometry

The best known type of geometry is of course the non-redundant case. A given number of non-redundant apertures n_A gives exactly $n_{UV} = n_A \times (n_A - 1)/2$ distinct uv sample points. Complete recovery of the wavefront φ requires $n_A - 1$ distinct constraints (the -1 comes from the fact that absolute phase reference is irrelevant), which leaves $n_K = n_{UV} - (n_A - 1) = (n_A - 1) \times (n_A - 2)/2$ additional pieces of information. The astute reader will have noted that this number exactly matches the expected number of closure triangles that can be formed with a n_A-aperture array.[14]

Another noteworthy configuration is the fully redundant hexagonal array, that is used to build large segmented telescopes such as Keck and JWST, or what is envisionned for TMT. These can be seen as a series of n_r concentric rings, usually with the central aperture missing. The total number of apertures, and matching number of distinct uv sample points are:

$$\begin{aligned} n_A &= 3n_r \times (n_r + 1) \\ n_{UV} &= 3n_r \times (2n_r + 1). \end{aligned} \tag{2}$$

Thus, a Keck-like array made of three concentric rings exhibits 36 segments and 63 distinct uv sample points. With two rings of segments, the JWST has 18 segments, 30 uv sample points. Except at the outermost positions of the pupil, removing apertures in the pupil leaves the number of distinct uv sample points unchanged, while it reduces the redundancy of the baselines in the array. Along with the distribution of redundancy in the uv plane, the difference between the number of uv sample points and the number of segments in the pupil conditions most of the imaging properties of an array. Section 4 explores the consequences of this observation to influence the design of arrays optimized for imaging.

2.3 Solving the linear problem... or not?

Analoguous to the classical image deconvolution problem, where both the object function and the point spread function (PSF) are unknown, the complete solution to Eq. 1 would be to uncover all n_{UV} components of the Φ_0 vector, that is all the accessible information about the target being observed, as well as the $n_A - 1$ components of φ. There are however never enough rows in $\mathbf{A}$ to allow for a complete solution.

Instead of solving the entire problem, the proposed approach is to extract useful information about the target, that does not depend on the wavefront error φ. This is achieved by identifying a left-hand operator $\mathbf{K}$ acting on Eq. 1 so that $\mathbf{K} \cdot \mathbf{A} = \mathbf{0}$, which gives:

$$\mathbf{K} \cdot \Phi = \mathbf{K} \cdot \Phi_0. \tag{3}$$

While some of the phase information Φ_0 appears to be lost in the process, one is left with a fraction of this original information, with the very useful property of not being affected by the pupil phase error φ: the kernel-phases. This of course borrows extensively from the idea of closure-phase.[11] The proposed formalism however allows to generalize and apply the idea to any imaging system, with no consideration for the redundancy of the array. In practice, the kernel-phase relations contained in the rows of $\mathbf{K}$ can be found as one of the results of the singular value decomposition (SVD) of the phase transfer matrix $\mathbf{A}$. The total number of kernel-phase relations n_K is given by the number of singular values of $\mathbf{A}$, and corresponds to the number of what were identified as extra rows in Section 2.3. If the SVD of $\mathbf{A}$ writes as: $\mathbf{A} = \mathbf{U}\mathbf{W}\mathbf{V}^T$, where $\mathbf{W}$ is a diagonal matrix containing the eigenvalues of $\mathbf{A}$, and $\mathbf{U}$ and $\mathbf{V}^T$ are unitary matrices, the kernel-phases relations themselves are made of

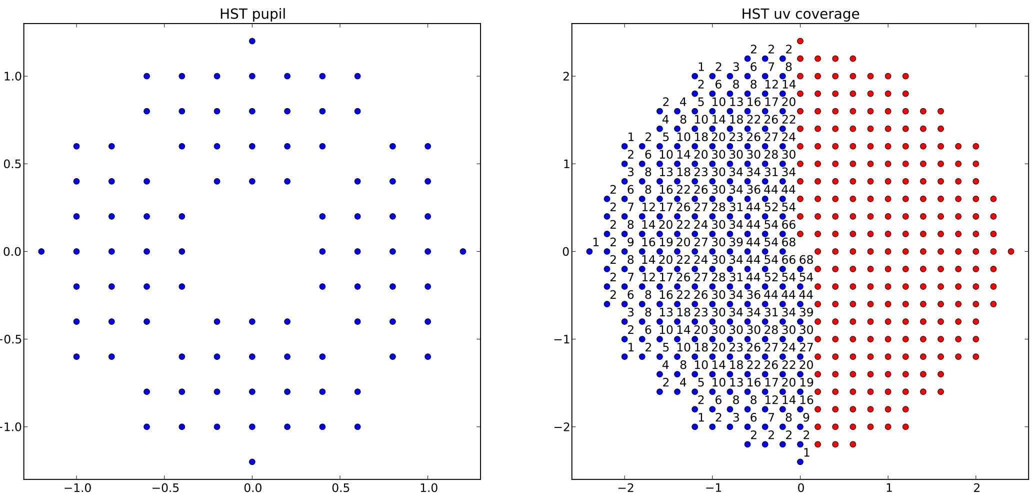

Figure 2. Left: Discretization of the HST pupil seen by NICMOS for the kernel-phase analysis. Right: resulting sampling in the uv plane. The number near each uv sample point indicates how redundant is each baseline.

the columns of $\mathbf{U}$ that correspond to zeros on the diagonal of $\mathbf{W}$. They form an orthonormal basis for the left null space (or kernel) of the phase transfer matrix, hence the name kernel-phase.

Not surprisingly, for a non-redundant array, the number of kernel-phases matches the expected number of closure-phases (cf. Section 2.2). Closure-phase appears as a special case of kernel-phase, where each relation involves only three apertures from the pupil. No serious advantage is therefore expected from using the general kernel-phase approach over the classical closure-phase in the non-redundant scenario, save for the orthogonality of the Ker-phases relations, which guarantees non-correlation of the signals (but does not address noise correlation), unlike the special closure-phase case, whose signals can be highly correlated.

For redundant apertures however, simple closure-phases are irrelevant, while kernel-phases do exist. The following section of this paper presents some of the results obtained from the kernel-phase data analysis of archival HST/NICMOS data.

3. HIGH CONTRAST BINARY DETECTION WITH KERNEL-PHASE

One of the most productive use of closure-phase with non-redundant masking interferometry has been the search for faint companions around a wide variety of targets.[1, 15–18] Since it takes advantage of the same self-calibrating property of closure-phase, and is targeted toward small inner working angles, one expects kernel-phase analysis of high Strehl images cover a very similar fraction of the parameter space, extending from ~ 0.5 to a few λ/D, beyond which image based detections are more appropriate. This section of the paper presents two science applications of the kernel-phase data analysis: first using snapshot images acquired with HST/NICMOS, and then using H-band AO-images acquired at the Subaru Telescope.

3.1 New binaries among nearby L-dwarfs

Non-saturated images acquired in the near infrared by NICMOS onboard HST such as the example image in Fig. 1 offer the ideal test case for this technique: the Strehl is quite high, and image quality excellent, with sampling better than Nyquist. We are proceeding to a revisit of a uniform sample of 77 ultracool M and L dwarfs observed in the course of two HST SNAPSHOT programs (GO 10143 and 10879). All targets were observed using the NIC1 camera and the F110W and F170M filters. From each snapshot, we expect sufficient sensitivity to companions with contrast $\sim 50:1$.

The first step in kernel-phase analysis is to build a discrete model of the pupil, and to determine the corresponding map of uv sampling points. Fig. 2 shows one possible model used for the HST pupil, made of 92

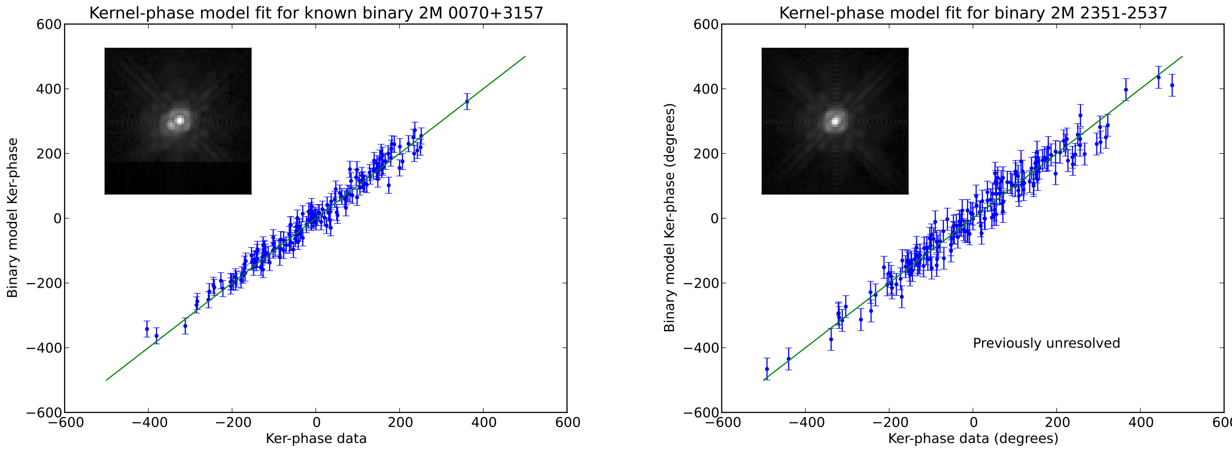

Figure 3. Examples of kernel-phase binary fit results on two ultracool dwarfs observed with HST/NIC1 in the F110W filter. Left: 2M 0070+3157 is a known binary, for which the companion was discovered from visual examination of the image. Right: 2M 2351-2537 is a previously unknown binary, that cannot be resolved in the direct image. The kernel-phase analysis produces a signal of comparable magnitude in either case.

elements falling on square grid pattern (left panel), along with the 212 distinct spatial frequencies they sample (right panel). All of this information, including the identity of the multiple baselines in the pupil that contribute to a single sample point in the uv plane, is encoded within the phase transfer matrix $\mathbf{A}$ introduced in Section 2, that is built from this model of the pupil only. The SVD of the phase transfer matrix produces the kernel-phases relations, which are used for the subsequent analysis.

The next step is to Fourier transform each of the frames, after careful centering and windowing of the image by a super-Gaussian function, so as to limit sensitivity to readout, and problems of aliasing, like usually done for non-redundant masking observations.[17] The phase of the Fourier transform is then sampled following the model resulting from the discretization of the pupil (cf. right panel of Fig. 1) and assembled into kernel-phases using the linear relations identified after the SVD. With this model of the HST pupil, each snapshot image leads to 166 kernel-phases. These are then used as input for a binary fit procedure that identifies the best binary fit in the (separation - position angle - contrast) parameter space, along with the uncertainties for each parameter. Fig. 3 presents the result of two such binary fit procedures (a previously known binary along with a newly discovered one). This simple 3-parameter model provides an excellent fit for this large number of observable quantities.

A preliminary kernel-phase analysis of this archival data exhibits two very clear detections of previously unknown companions around 2M 2351-2537 and 2M 2028+0052 (Pope et al, 2012, *in prep*). The properties of the best binary fit for both targets in both filters are summarized in Table 1.

Table 1. Best parameter fit for newly discovered ultracool dwarfs binaries after kernel-phase analysis of HST archival data. Angular separation for these objects are well inside the formal diffraction limit of the HST in the near infrared.

2MASS identifier	**Filter**	**Separation (mas)**	**Position Angle (degrees)**	**Contrast**
2028+0052	F170M	54.7 $\pm$ 10.8	111.9 $\pm$ 3.6	1.37 $\pm$ 0.28
	F110W	42.3 $\pm$ 2.8	121.3 $\pm$ 3.0	4.7 $\pm$ 2.4
2351-2537	F170M	71.9 $\pm$ 3.2	353.6 $\pm$ 3.0	1.57 $\pm$ 0.27
	F110W	66.0 $\pm$ 3.6	347.4 $\pm$ 2.5	2.97 $\pm$ 0.7

Note that for the F110W and F170M filters, the diffraction limit of HST respectively lies at 88 and 136 milliarcseconds. The two detections reported in Table 1 exhibit angular separations $\sim 0.5\lambda/D$ or smaller, showing that the technique indeed opens up access to the super-resolution regime. For these very small angular

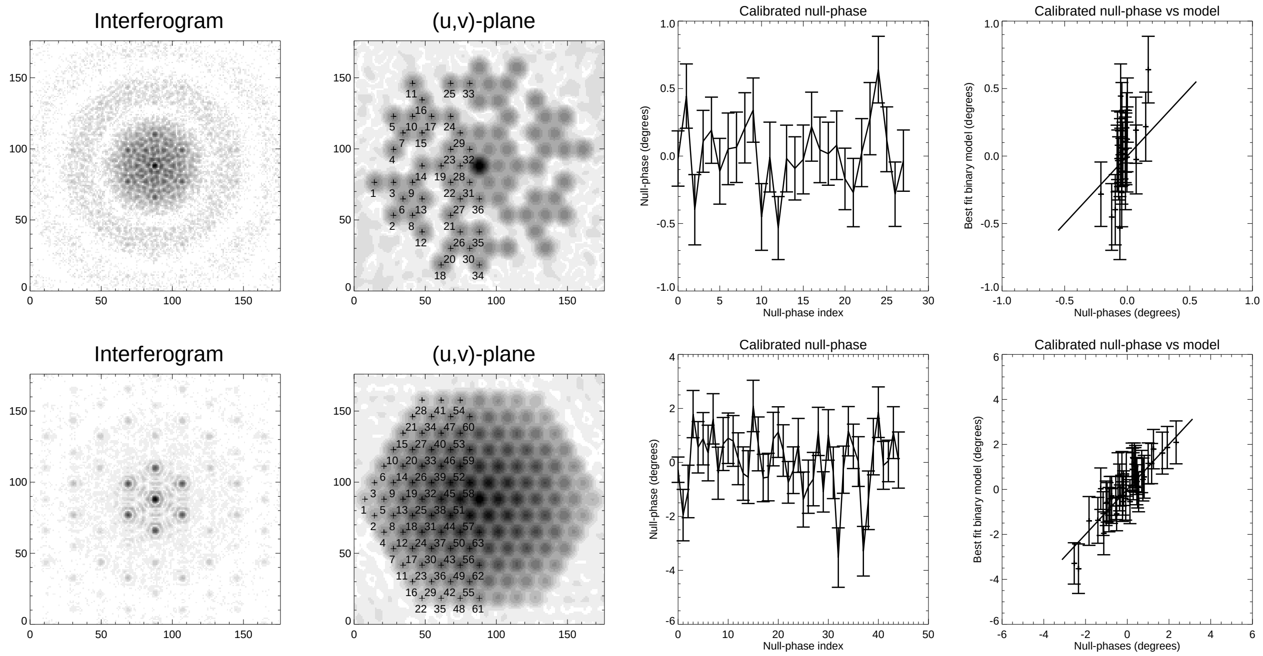

Figure 4. Example of numerical simulation comparing high contrast detection performance of a NRM-interferometry (top row) closure-phase data set and a redundant aperture kernel-phase (bottom row) data set acquired under the same simulated observing conditions. From left to right, both rows show one example of interferogram, the matching uv-coverage, the final calibrated data product (closure- or kernel-phase), and a binary fit.

separations, even with non-redundant masking interferometry, contrast and angular separation are expected to be highly correlated[19] and therefore hard to constrain. Despite being well inside this challenging region of the parameter space, and resulting from the analysis of one single frame per filter, the agreement between the parameters for both filters is remarkable. In addition to these two clear detections, our analysis also seems to indicate the presence of five additional binary candidates at lower confidence. Additional Monte Carlo simulations are required to conclude upon the actual existence of these eluding very close companions.

3.2 Ground based AO kernel-phase developments

While NRM interferometry behind AO has managed in less than 10 years to become a somewhat mainstream technique, a demonstration of the relevance of kernel-phase to ground-based AO observations still has to happen. With the ever improving overall level of AO correction, and particularly with the emergence of the so-called extreme-AO systems that promise to deliver very high Strehl ratios (> 90 %), kernel-phase on full-pupil images is expected to become a very useful technique for high contrast at the detection limit. In the high Strehl regime, because it benefits from the same self-calibration trick as closure-phase acquired in NRM-interferometry, full-pupil kernel-phase is expected to perform at least as well as its sparse counterpart.

Figure 3.2 presents the results of some simulations that argue in this direction, and in fact suggest that kernel-phase outperforms the NRM-interferometry closure-phase for high contrast detection. For both simulations, a 7-magnitude contrast binary was simulated at angular separation $\sim 1.5\lambda/D$. A direct comparison of the calibrated data against the model of the known binary (rightmost plots in Fig. 3.2) shows that the kernel-phase redundant aperture data better matches the model. Complementary analysis of the full 3-D χ^2 space confirms that a convincing detection is possible with the full-aperture kernel-phase, but not with the NRM closure-phase.

The Keck Observatory Archive (KOA) recently opened access to large amounts of NIRC2 AO. The development of a reliable and robust data-reduction pipeline compatible with NIRC2 (in addition to the existing NICMOS1 data (cf. 3.1) is ongoing and will allow the re-analysis of relevant data, in a manner comparable to what is already ongoing with HST/NICMOS1 data.

4. REDUNDANT IMAGING ARRAYS

The design of interferometric masks for imaging has so far been guided by the widely used designs of Golay,[20] who provides a series of compact solutions using three-fold symmetry, that maximize the uv coverage while ensuring non-redundancy. These guidelines of Golay have ruled the design of non-redundant masks on all major telescopes where this observing mode is available, save for a few adjustments imposed by specific constraints due to the geometry of the pupil, as well as the bandwidth of the filters they are intented to be used with. With kernel-phase, we have seen that non-redundancy of the pupil is no longer mandatory to ensure the extraction of self-calibrating observable quantities: this newly gained freedom permits the design of possibly improved arrays, optimized for the imaging of complex sources, which is what this section of the paper proposes to present.

The imaging of complex sources with an interferometric array requires a good coverage of the uv plane. While it is always possible to increase this coverage with aperture synthesis technique that use telescope roll (or sky rotation), this discussion will be restricted to the possibility of imaging a complex source from a single snapshot Fizeau image only, such as what would be acquired with a mask in the pupil of an instrument behind AO. The imaging capability is entirely dictated by the total number of independent observables (visibilities and kernel-phases) that can be extracted from the snapshot.

The compact G12 array (cf. top panel of Fig. 4) is one example of compact 12-aperture array geometry proposed by Golay,[20] with apertures falling on a regular hexagonal grid. Being non-redundant, this array therefore allows to sample $12 \times (12-1)/2 = 66$ distinct uv sample points, and produce $(12-1) \times (12-2)/2 = 55$ kernel-phases.

Given that such a non-redundant mask needs to fit inside the pupil of an existing instrument, it seems fair to compare it to a fully redundant configuration that fits within the same global footprint. In addition, all apertures should fall upon the same regular hexagonal grid, so that the smallest and longest baselines that respectively define the size of the field of view of the array and its resolution, remain unchanged. With this configuration, the uv-coverage increases significantly as the total number of distinct uv sample points reaches 108 (cf. middle panel of Fig. 4). While classical closure-phase relations cannot be constructed for this highly redundant configuration, the SVD of the corresponding transfer matrix (cf. Sec. 2) reveals that only 45 kernel-phases can be extracted from this array.

A much more interesting alternative to the fully-redundant array is to keep only the outermost apertures as shown in the lower panel of Fig. 4. This "ring" configuration provides the same total uv coverage as the fully redundant aperture with 108 distinct sample points. The SVD of this new sparser transfer matrix uncovers 85 kernel-phases, which is a significant improvement over the G12 geometry.

	Golay 12	**Full**	**Ring**
n_A	12	27	15
f_A	0.61 (N_{UV}=66)	1.0 (N_{UV}=108)	1.0 (N_{UV}=108)
f_R	0.83 (N_K=55)	0.45 (N_K=49)	0.79 (N_K=85)
$f_A \times f_R$	0.51	0.45	0.79

Table 2. Summary of the imaging properties of the Golay 12, Full and Ring configurations presented in Fig. 4. n_A, n_{UV} and n_K respectively represent the total number of apertures in the array, the number of distinct uv samples they offer access to and the number of kernel-phases that can be assembled from these measurements. f_A and f_R respectively represent the fraction of available and recoverable uv information. The ring configuration shows a very net advantage over the two other configurations.

The properties of these three different configuration are summarized in Table 4. The total fraction of phase information that is recovered by the considered geometries depends on the total number of uv-points, (100 % for the full and ring configurations), and the number of kernel-phases that can be extracted from data acquired by one such array. While only one single Golay array (compact Golay 12) is used here as the starting point, the observations remain essentially unchanged for other geometries. The ring configuration systematically produces

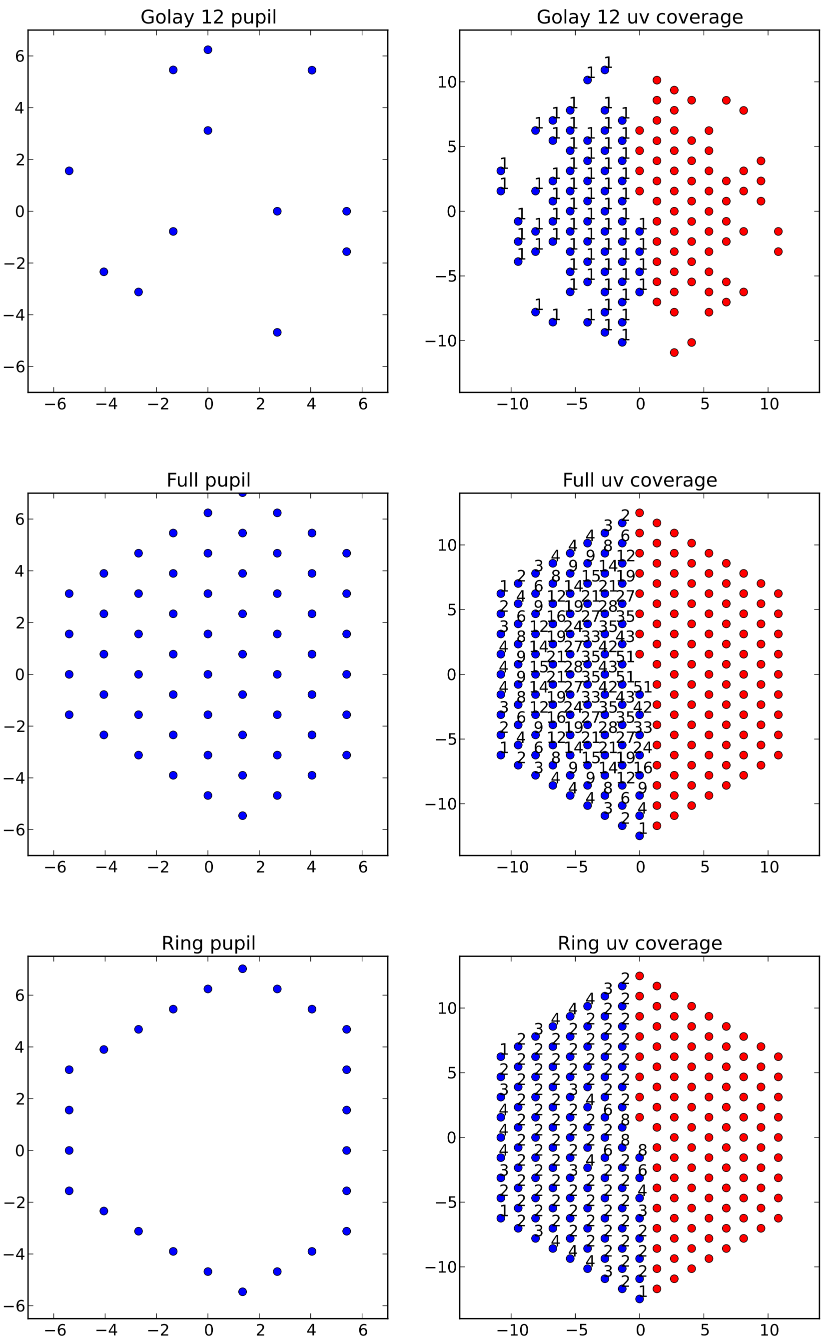

Figure 5. Comparison of the Golay 12 compact configuration with two redundant alternative that fit within the same footprint. The left column presents the pupil geometries and the right columnm, their respective coverage of the uv plane.

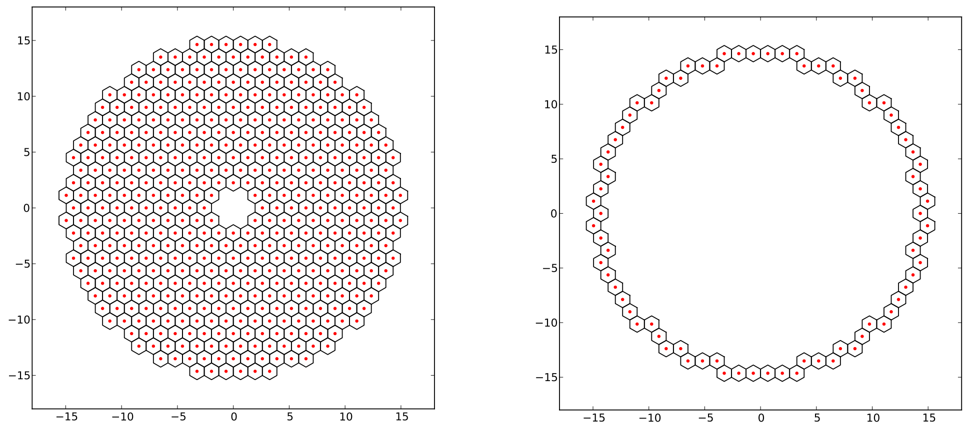

Figure 6. Left: geometry for the 492 segments of the Thirty Meter Telescope (TMT). Right: geometry of the 78 outermost segments that provide access to the same identical uv coverage. Properties of both configurations are summarized in Table 4.

the highest phase information recovery rate (here 79 %), outperforming the two other configurations by a factor ~ 1.5.

This fraction increases with the number of apertures and the symmetry in the geometry of their relative arrangement. If one looks a little ahead at what this type of reasoning would give on a large telescope, say the Thirty Meter Telescope (TMT, cf. Table 4), a ring configuration becomes extremely compelling. Only 78 segments on the outermost ring provide access to the same uv-coverage (972 distinct uv samples) as the original pupil. In addition, the arrangement of these 78 segments alone allow to produce a very large number of kernel-phases (933), suggesting that 96 % of the total available phase information can be recovered.

Table 3. Imaging properties of the full and outer ring only pupil configurations for the TMT mirror, shown in Fig. 6. Despite having 6 times as few segments as the full configuration, the ring geometry exhibits the same uv-coverage and permits the extraction of a higher number of kernel-phases.

	Full pupil	**Ring only**
n_A	492	78
n_{UV}	972	972
n_K	726 (75 %)	933 (96 %)
Max. redundancy	462	26
Mean redundancy	124	3

Moreover, in the ring configuration, both the maximal and mean redundancy of the pupil are reduced by a factor > 10. While the redundancy is encoded in the kernel-phase, the robustness to larger phasing errors is expected to increase as the redundancy decreases. A ring mask inserted in the pupil of an ELT may turn out as a relevant option for a first generation AO instrument.

5. WAVEFRONT SENSING

The proposed formalism can also be used as a basis to understand some aspects of the wavefront sensing problem. Looking back at Eq. 1, solving for the wavefront requires to invert the relation:

$$\varphi = \mathbf{A^{-1}} \cdot (\Phi - \Phi_O), \tag{4}$$

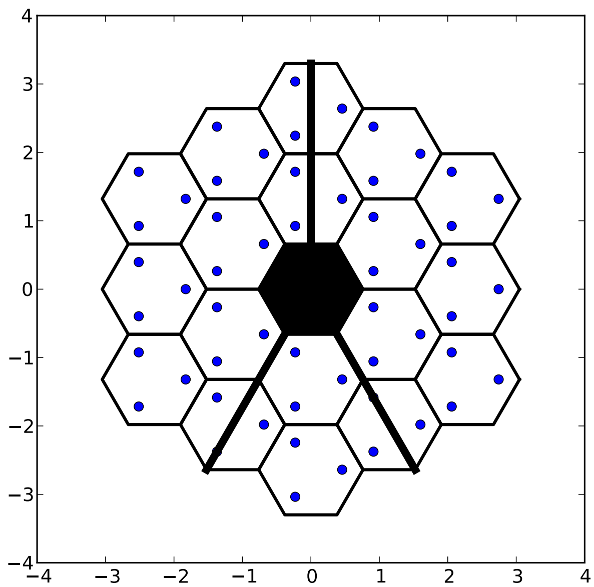

Figure 7. Example of interferometric mask suited to the wavefront sensing for a segmented telescope such as JWST. Properties of the phase transfer matrix $\mathbf{A}$ for this mask show that tip-tilt and piston for each segment can be recovered from the analysis of a single focal plane image.

where $\mathbf{A^{-1}}$ is a pseudo-inverse of $\mathbf{A}$, that can also be build from the SVD of $\mathbf{A}$. For wavefront sensing purposes, the target true phase term Φ_O is a nuisance parameter, that requires some calibration. We can assume for now that the target is non resolved and contains no phase structure ($\Phi_O = 0$).

Whether the pseudo-inverse proves useful or not, depends on the total number of non-singular values of $\mathbf{A}$, which as is now obvious, is entirely dependent upon the geometry of the pupil. Except for the special case of a non-redundant aperture, the wavefront sensing problem for a conventional aperture is however known to be degenerate. Starting from a fully-redundant pupil, it takes very little modification of the geometry to make the problem directly invertible. A more thorough treatement of this case will be the object of future work, but Fig. 7 shows one example of geometry that, although redundant, is adapted to the wavefront sensing of a segmented mirror.

This is of course of special interest in the context of extreme AO systems that require the calibration of the non-common path error between the science camera and the wavefront sensor. This operation typically requires either a long acquisition sequences, while moving an optical element like in phase diversity (PALM-3000 on Palomar or SCExAO on Subaru), or a dedicated interferometric calibration unit (like in the Gemini Planet Imager). Because this error is small, with a well chosen pupil mask, a very good estimate of the non-common path error may be measured from the analysis of a single focal plane image.

6. CONCLUSION

Kernel-phase is no longer just applicable to almost ideal near-IR images by HST but also relevant to today's AO images. Very little science has come from the application of the technique yet, but the availability of large on-line archives makes it possible to post-process a lot of data, to extract new science results: even before new observing time is allocated explicitly for the technique, one should expect some interesting results to come out within the next year.

The easiest and maybe most rewarding application of the technique is the detection of high contrast companions at the diffraction limit. A revisit of HST/NICMOS archival data on nearby ultracool dwarfs is now under way, and will provide new results with improved astrometry and detection limits. In addition, high-Strehl AO simulations comparable to what extreme AO systems are becoming able to deliver, actually suggest that full-pupil kernel-phase data analysis demonstrates better sensitivity than NRM-interferometry closure-phase in identical observing conditions.

Because it frees from the constraint of non-redundancy, kernel-phase also permits to work with array geometries that optimize phase information recovery rate. In this context, ring shaped masks do seem to provide very close to an optimal configuration. In addition to usual NRM (Golay-type) masks, ring masks should be thought of as a useful gizmo to include as part of the offering of all modern AO instruments. Finally, through analysis of the properties of the phase transfer matrix, it seems possible to produce pupil masks that although redundant, can even be used for focal plane based wavefront sensing purposes.

The ideas presented in this work entirely rely on a linear model, that is only applicable when wavefront errors are small. The wide availability of high quality ground based AO systems and the arrival of extreme AO systems however make this model relevant to a fair fraction of today's AO observations: just as NRM-interferometry has progressively managed to become a somewhat mainstream observing technique, kernel-phase is likely to become a powerful and widely used tool for high contrast imaging.

REFERENCES

[1] Kraus, A. L. and Ireland, M. J., "LkCa 15: A Young Exoplanet Caught at Formation?," ApJ **745**, 5 (Jan. 2012).

[2] Biller, B., Lacour, S., Juhász, A., Benisty, M., Chauvin, G., Olofsson, J., Pott, J.-U., Müller, A., Sicilia-Aguilar, A., Bonnefoy, M., Tuthill, P., Thebault, P., Henning, T., and Crida, A., "A Likely Close-In Low-Mass Stellar Companion to the Transitional Disk Star HD 142527," *ArXiv e-prints* (June 2012).

[3] Marois, C., Lafrenière, D., Doyon, R., Macintosh, B., and Nadeau, D., "Angular Differential Imaging: A Powerful High-Contrast Imaging Technique," ApJ **641**, 556–564 (Apr. 2006).

[4] Malbet, F., Yu, J. W., and Shao, M., "High-Dynamic-Range Imaging Using a Deformable Mirror for Space Coronography," PASP **107**, 386 (Apr. 1995).

[5] Guyon, O., Pluzhnik, E., Martinache, F., Totems, J., Tanaka, S., Matsuo, T., Blain, C., and Belikov, R., "High-Contrast Imaging and Wavefront Control with a PIAA Coronagraph: Laboratory System Validation," PASP **122**, 71–84 (Jan. 2010).

[6] Martinache, F., Guyon, O., Clergeon, C., and Blain, C., "Speckle Control with a remapped-pupil PIAA-coronagraph," *ArXiv e-prints* (June 2012).

[7] Readhead, A. C. S., Nakajima, T. S., Pearson, T. J., Neugebauer, G., Oke, J. B., and Sargent, W. L. W., "Diffraction-limited imaging with ground-based optical telescopes," AJ **95**, 1278–1296 (Apr. 1988).

[8] Nakajima, T., Kulkarni, S. R., Gorham, P. W., Ghez, A. M., Neugebauer, G., Oke, J. B., Prince, T. A., and Readhead, A. C. S., "Diffraction-limited imaging. II - Optical aperture-synthesis imaging of two binary stars," AJ **97**, 1510–1521 (May 1989).

[9] Tuthill, P. G., Monnier, J. D., Danchi, W. C., Wishnow, E. H., and Haniff, C. A., "Michelson Interferometry with the Keck I Telescope," PASP **112**, 555–565 (Apr. 2000).

[10] Tuthill, P., Lloyd, J., Ireland, M., Martinache, F., Monnier, J., Woodruff, H., ten Brummelaar, T., Turner, N., and Townes, C., "Sparse-aperture adaptive optics," in [*Advances in Adaptive Optics II. Edited by Ellerbroek, Brent L.; Bonaccini Calia, Domenico. Proceedings of the SPIE, Volume 6272, pp. (2006).*], (July 2006).

[11] Jennison, R. C., "A phase sensitive interferometer technique for the measurement of the Fourier transforms of spatial brightness distributions of small angular extent," MNRAS **118**, 276–+ (1958).

[12] Martinache, F., "Kernel Phase in Fizeau Interferometry," ApJ **724**, 464–469 (Nov. 2010).

[13] Martinache, F., "Kernel-phases for high-contrast detection beyond the resolution limit," in [*Society of Photo-Optical Instrumentation Engineers (SPIE) Conference Series*], *Society of Photo-Optical Instrumentation Engineers (SPIE) Conference Series* **8151** (Sept. 2011).

[14] Monnier, J. D., "An Introduction to Closure Phases," in [*Principles of Long Baseline Stellar Interferometry*], Lawson, P. R., ed., 203–+ (2000).

[15] Kraus, A. L., Ireland, M. J., Martinache, F., and Lloyd, J. P., "Mapping the Shores of the Brown Dwarf Desert. I. Upper Scorpius," ApJ **679**, 762–782 (May 2008).

[16] Kraus, A. L., Ireland, M. J., Martinache, F., and Hillenbrand, L. A., "Mapping the Shores of the Brown Dwarf Desert. II. Multiple Star Formation in Taurus-Auriga," ApJ **731**, 8 (Apr. 2011).

[17] Ireland, M. J., Kraus, A., Martinache, F., Lloyd, J. P., and Tuthill, P. G., "Dynamical Mass of GJ 802B: A Brown Dwarf in a Triple System," ApJ **678**, 463–471 (May 2008).

[18] Ireland, M. J. and Kraus, A. L., "The Disk Around CoKu Tauri/4: Circumbinary, Not Transitional," ApJ **678**, L59–L62 (May 2008).

[19] Martinache, F., Rojas-Ayala, B., Ireland, M. J., Lloyd, J. P., and Tuthill, P. G., "Visual Orbit of the Low-Mass Binary GJ 164 AB," ApJ **695**, 1183–1190 (Apr. 2009).

[20] Golay, M., "Point arrays having compact, nonredundant autocorrelations," *JOSA* **61**, 272–273 (1971).